



# Bacterial Cyclodipeptides Target Signal Pathways Involved in Malignant Melanoma

Mayra Xóchitl Durán-Maldonado<sup>1</sup>, Laura Hernández-Padilla<sup>1</sup>, Juan Carlos Gallardo-Pérez<sup>2</sup>, Alma Laura Díaz-Pérez<sup>1</sup>, Lorena Martínez-Alcantar<sup>1</sup>, Homero Reyes De la Cruz<sup>3</sup>, José Salud Rodríguez-Zavala<sup>2</sup>, Gustavo Pacheco-Rodríguez<sup>4</sup>, Joel Moss<sup>4</sup> and Jesús Campos-García<sup>1\*</sup>

<sup>1</sup> Laboratorio de Biotecnología Microbiana, Instituto de Investigaciones Químico-Biológicas, Universidad Michoacana de San Nicolás de Hidalgo, Morelia, Mexico, <sup>2</sup> Departamento de Bioquímica, Instituto Nacional de Cardiología, Mexico City, Mexico, <sup>3</sup> Laboratorio de Control Traduccional, Instituto de Investigaciones Químico-Biológicas, Universidad Michoacana de San Nicolás de Hidalgo, Morelia, Mexico, <sup>4</sup> Pulmonary Branch, National Heart, Lung, and Blood Institute, National Institutes of Health, Bethesda, MD, United States

## OPEN ACCESS

### Edited by:

Nihal Ahmad,  
University of Wisconsin-Madison,  
United States

### Reviewed by:

Gagan Chhabra,  
University of Wisconsin-Madison,  
United States  
Jasmine George,  
Medical College of Wisconsin,  
United States

### \*Correspondence:

Jesús Campos-García  
jcgarcia@umich.mx

### Specialty section:

This article was submitted to  
Skin Cancer,  
a section of the journal  
Frontiers in Oncology

**Received:** 20 February 2020

**Accepted:** 03 June 2020

**Published:** 24 July 2020

### Citation:

Durán-Maldonado MX, Hernández-Padilla L, Gallardo-Pérez JC, Díaz-Pérez AL, Martínez-Alcantar L, Reyes De la Cruz H, Rodríguez-Zavala JS, Pacheco-Rodríguez G, Moss J and Campos-García J (2020) Bacterial Cyclodipeptides Target Signal Pathways Involved in Malignant Melanoma. *Front. Oncol.* 10:1111. doi: 10.3389/fonc.2020.01111

Melanoma is an aggressive cancer that utilizes multiple signaling pathways, including those that involve oncogenes, proto-oncogenes, and tumor suppressors. It has been suggested that melanoma formation requires cross-talk of the PI3K/Akt/mTOR and Ras-ERK pathways. This pathway cross-talk has been associated with aggressiveness, drug resistance, and metastasis; thus, simultaneous targeting of components of the different pathways involved in melanoma may aid in therapy. We have previously reported that bacterial cyclodipeptides (CDPs) are cytotoxic to HeLa cells and inhibit Akt phosphorylation. Here, we show that CDPs decreased melanoma size and tumor formation in a subcutaneous xenografted mouse melanoma model. In fact, CDPs accelerated death of B16-F0 murine melanoma cells. In mice, antitumor effect was improved by treatment with CDPs using cyclodextrins as drug vehicle. In tumors, CDPs caused nuclear fragmentation and changed the expression of the Bcl-2 and Ki67 apoptotic markers and promoted restoration of hyperactivation of the PI3K/Akt/mTOR pathway. Additionally, elements of several signaling pathways such as the Ras-ERK, PI3K/JNK/PKA, p27Kip1/CDK1/survivin, MAPK, HIF-1, epithelial-mesenchymal transition, and cancer stem cell pathways were also modified by treatment of xenografted melanoma mice with CDPs. The findings indicate that the multiple signaling pathways implicated in aggressiveness of the murine B16-F0 melanoma line are targeted by the bacterial CDPs. Molecular modeling of CDPs with protein kinases involved in neoplastic processes suggested that these compounds could indeed interact with the active site of the enzymes. The results suggest that CDPs may be considered as potential antineoplastic drugs, interfering with multiple pathways involved in tumor formation and progression.

**Keywords:** antitumor activity, cyclodipeptides, tumorigenesis, melanoma, cell proliferation, apoptosis, epithelial-mesenchymal transition

## INTRODUCTION

Communication between the microbiome and host cells plays important roles in health and disease (1). Microbes produce metabolites capable of affecting cellular signaling pathways and thus could become potent therapeutics (2). For instance, structurally diverse cyclodipeptides (CDPs) of bacterial (3, 4) and with less efficiency of synthetic origin (5) are cytotoxic to human cancer cell lines. In fact, we have shown that CDPs [cyclo(L-Pro-L-Tyr), cyclo(L-Pro-L-Val), and cyclo(L-Pro-L-Phe)] from *Pseudomonas aeruginosa* PAO1 promoted apoptosis and cell death of human cervical (HeLa) and colorectal adenocarcinoma (CaCo-2) cells, whereas normal human lung fibroblasts were insensitive (6). The molecular mechanisms used by CDPs to trigger cytotoxicity, leading to death of cancer cells, appear to involve microtubule polymerization (7) and caspase-3 activation (3, 6).

Cancer results from dysfunction of fundamental cellular processes. In fact, pathways involving oncogenes and tumor suppressors are frequently involved in cancer development and progression (8, 9). Interestingly, the mechanistic target of rapamycin (mTOR) serine/threonine kinase is a master regulator that participates in two complexes (mTORC1 and mTORC2), and its dysregulation has been implicated in cancer. mTORC1 has been implicated in cellular processes, such as, energy metabolism, proliferation, tumorigenesis, and autophagy, whereas the mTORC2 complex is involved in actin cytoskeleton reorganization and survival (10). mTORC1 activity is frequently up-regulated in cancer, particularly following increased oncogenic activation of phosphoinositide 3-kinase (PI3K) signaling or inactivation of the lipid phosphatase PTEN (phosphatase and tensin homolog) (9, 11).

Multiple biomarkers characterize a neoplasm/cancer and metastasis (9, 10, 12), which in many cases is initiated by cancer stem cells (CSC) and may involve epithelial-mesenchymal transition (EMT). Epithelial-mesenchymal transition has been associated with action of N-cadherin, a membrane protein involved in cell attachment, which is up-regulated during metastasis and invasion, and promotes tumorigenesis. Additionally, direct interaction of N-cadherin with PI3K may enable activation of the PKB/Akt pathway, suggesting that it could be a therapeutic target in cancer (13). N-cadherin can also promote cell survival, migration/invasion, and the EMT process by direct cross-talk with other signaling pathways, [e.g., nuclear factor  $\kappa$ B (NF $\kappa$ B)-mediated, mitogen-activated protein kinase (MAPK), receptor tyrosine kinase (RTK), Ras homolog family member A small GTPase protein (RhoA GTPase), PI3K (14)]. Otherwise, EMT is a crucial regulatory pathway with links to embryogenesis and cancer development.

In melanoma, multiple signaling pathways are dysregulated, involving oncogenes and tumor suppressors (i.e., PI3K/AKT/mTOR, MAPK, RAS/MEK/ERK, BRAF, and CDK); the multiple dysregulation of these signaling pathways favors tumor invasiveness, progression, drug resistance, and recurrence. Current therapeutic procedures for melanoma include chemotherapy, immunotherapy, biochemotherapy, and gene therapy (15, 16). However, participation of multiple

signaling pathways in melanoma pathology complicates its treatment. Then, the elucidation of the involvement of EMT and CSC pathways in melanoma invasiveness, drug resistance, and recurrence is crucial. The main goal of this study was to evaluate the effects of CDPs on a xenografted melanoma tumor model and elucidate the molecular mechanisms involved in CDP action. We observed that CDPs killed melanoma cells and decreased tumor burden. During melanoma development, multiple cell-signaling pathways were targeted and restored by bacterial CDPs, suggesting that these molecules have the potential for use as antiproliferative drugs.

## MATERIALS AND METHODS

### Chemicals and Reagents

Dulbecco modified Eagle medium (DMEM), fetal bovine serum (FBS), 3-(4,5-dimethylthiazol-2-yl)-2,5-diphenyltetrazolium bromide (MTT), and  $\beta$ -cyclodextrin ( $\beta$ -cyclodextrin hydrate) were purchased from Sigma-Aldrich Co., St. Louis, MO, USA). Alexa Fluor 488 annexin V and the propidium iodide (PI)/dead cell apoptosis kits were from Invitrogen Life Technologies, Carlsbad, CA, USA. Cyclodipeptides were obtained from *P. aeruginosa* PAO1 and characterized as previously described (17, 18).

### Cell Culture

Mouse B16-F0 melanoma cells line was obtained from the American Type Culture Collection (ATCC, Manassas, VA, USA). Cells were cultured in complete media (CM) [DMEM supplemented with 10% (vol/vol) FBS, 100 U/mL of penicillin, 40  $\mu$ g/mL of streptomycin, and 1  $\mu$ g/mL of amphotericin B (Sigma-Aldrich Co., St. Louis, MO, USA)]. Cell culture media were changed twice a week and maintained at 37°C under 80% humidity and incubated in an atmosphere of 5% CO<sub>2</sub>. Following trypsinization, cells were grown to confluency; cells were counted using a hemocytometer chamber.

### Cell Viability, Necrosis, and Apoptosis Assays

Cell viability was determined colorimetrically with MTT. Briefly, cells were seeded in 96-well flat-bottomed plates at a density of  $3 \times 10^4$  cells per well in 200  $\mu$ L of CM medium and incubated by 24 h at 37°C with 5% CO<sub>2</sub> as described above. Then, cell culture media were removed and replaced with serum-free DMEM. Following incubation in DMEM with FBS for 24 h, cells were incubated in the presence or absence of the indicated amounts of CDPs for 24 h at 37°C with 5% CO<sub>2</sub>. To determine cell viability, MTT, 50 mg/mL in phosphate-buffered saline (PBS), was added to each well and incubated for 4 h at 37°C. Finally, 100  $\mu$ L of 2-propanol/1 M HCl (19:1 vol/vol) was added to dissolve formazan crystals, and absorbance was measured at 595 nm using a microplate reader (BioTek Instruments, Winooski, VT, USA).

To quantify necrosis and apoptosis, cell cultures were incubated with DMEM with FBS for 12 h prior to treatment with CDPs. Dimethyl sulfoxide (DMSO) was used as a control at the same concentration used to dissolve the CDPs. Following incubation, cells were collected by centrifugation at 2,000 g for

10 min. The pellet was suspended in 20  $\mu\text{L}$  and incubated with annexin V and propidium iodide (PI) (Dead Cell Apoptosis Kit; Molecular Probes, Invitrogen Life Technologies, Carlsbad, CA, USA). Fluorescence was immediately quantified by fluorescence-activated cell sorting (FACS) using an Accuri-C6 Flow Cytometer (BD Biosciences, San Jose, CA, USA). The percentages of fluorescent cells (PFC) and median fluorescence intensity were determined from histograms of the fluorescence emission in the plots, labeled as PFC or as relative fluorescence units. For apoptosis and necrosis assays, annexin V fluorescence was measured with fluorescence channel FL1 at 495/519 nm and for PI in FL2 channel at 535/617 nm. At least 20,000 cellular events were used for calculations.

## Subcutaneous Xenografted Melanoma Mouse Model

All the experiments using mice complied with standard guidelines for the welfare of animals with experimental neoplasia in accordance with the recommendations of the Mexican Official Regulations for the Use and Care of Animals (NOM 062-ZOO-1999; Ministry of Agriculture, Mexico). This research was also approved by the Institutional Committee for Use of Animals of the Universidad Michoacana de San Nicolás de Hidalgo. Male C57BL/6 mice between the ages of 4 and 5 weeks were purchased from Envigo RMS S.A. (Mexico City, Mexico). Animals were hosted in facilities for 2 weeks before experiments were started; afterward, the xenograft melanoma procedure was conducted as described below. The mice were housed separately in ventilated cages under a controlled light cycle (12-h light/12-h dark) at room temperature (22–26°C) and were fed with a standard rodent diet and water *ad libitum* in accordance with NOM 062-ZOO-1999; Ministry of Agriculture, Mexico.

Melanoma cells were injected subcutaneously in mice at the right flank with  $2 \times 10^5$  B16-F0 murine melanoma cells. Tumor size was measured every 2 days. Two bisecting diameters of each tumor were measured with calipers. The volume was calculated using the formula  $(0.4)(ab^2)$ , with “a” being the larger diameter and “b” being the smaller diameter (19). All mice injected with melanoma cells developed tumors of 20–50  $\text{mm}^3$  8 days from the day of injection. The CDPs were administered at a dose of 0.1 mg/g of mice weight, which was determined assuming that the corporal volume of mice is  $\sim 50 \text{ cm}^2$ . A concentration of 50  $\mu\text{g}/\text{mL}$  (50% apoptotic cells in the assay) was used, rendering 2.5 mg per mouse per dose. In addition, two additional doses of CDPs were tested in a pilot study, with CDP treatment at 10, 50, and 200  $\mu\text{g}/\text{mL}$  of CDPs. The results showed similar antitumorigenic effect at 50 and 200  $\mu\text{g}/\text{mL}$  of CDPs, but no significant results with 10  $\mu\text{g}/\text{mL}$  of CDPs; thus, we decided to use 50  $\mu\text{g}/\text{mL}$  of CDPs for this study. A 50 mg/mL stock solution of CDPs was prepared by dissolving the compounds in sterile saline solution containing DMSO (0.1 %), or  $\beta$ -cyclodextrin (50 mg/mL). All liquid treatments of the mouse model were injected in the caudal vein as authorized by NOM 062-ZOO-1999; Ministry of Agriculture, Mexico. Seven different groups of six mice each were randomly assigned: (1) control, healthy mice were injected with 50  $\mu\text{L}$  of sterile saline solution with DMSO (0.1%);

(2) control + CDPs, healthy mouse group injected with 50  $\mu\text{L}$  of CDP stock solution; (3) tumor (T), mice with melanoma tumors were injected with 50  $\mu\text{L}$  of sterile saline solution with DMSO (0.1%); (4) T + CDPs-t0, mice with melanoma cell injections were treated from the beginning with a weekly injection with 50  $\mu\text{L}$  of CDP stock solution (three total doses); (5) T + CDPs-t8, mice with melanoma tumors (with volume of  $\sim 20$ – $50 \text{ mm}^3$  after 8 days) were injected weekly with 50  $\mu\text{L}$  of CDP stock solution (two total doses); (6) T + CDPs-cdxt0, mice as in group 4 were injected weekly with 50  $\mu\text{L}$  of CDP stock solution in  $\beta$ -cyclodextrins (50 mg/mL, three total doses); and (7) T + CDPs-cdxt8 mice as in group 5 were treated weekly with 50  $\mu\text{L}$  of CDP stock solution in  $\beta$ -cyclodextrin (50 mg/mL, two total doses). The mice were examined every 2 days and weighed, and tumor size was measured until they were euthanized (20 days) as authorized by the Institutional Committee for Use of Animal of the Universidad Michoacana de San Nicolás de Hidalgo in accord to the NOM 062-ZOO-1999; Ministry of Agriculture, Mexico. Then, organs were removed, tumor area was determined, and dissected tumors and organs were stored at  $-80^\circ\text{C}$  prior to histopathological studies. Mice that died of causes unrelated to the neoplasm and CDP treatment were not considered in the analysis.

## Blood Parameters Evaluation

Blood was obtained by cardiac puncture prior to euthanizing as recommended (NOM 062-ZOO-1999; Ministry of Agriculture, Mexico) and collected in tubes containing heparin. Blood was centrifuged at 3,500 g for 10 min to obtain plasma. Hematocrit was measured by centrifugation (10,000 g for 5 min) using a hematocrit capillary tube. Hemoglobin was determined as follows:  $\text{Hb} = (\text{hematocrit value}) (3.3 \text{ factor})$ . Plasma was utilized to measure lactate dehydrogenase (LDH), aspartate aminotransferase (AST), and alanine aminotransferase (ALT) activities using the Dry Chemical Analyzer Vitros 350 (Ortho Clinical Diagnostics, Wooburn Green, Buckinghamshire, UK).

## Histological Analysis of Tumor Tissue

Tumors and tissues from mice were excised and fixed in 10% neutral-buffered formaldehyde solution and embedded in paraffin. Tissue sections (0.2 mm  $\times$  10  $\mu\text{m}$ ) were obtained using a Cryostat (Leica CM1850, Leica Biosystems Inc., Buffalo Grove, IL, USA) and stained with hematoxylin-eosin. For immunohistochemical analysis, formalin-fixed tissue sections were dehydrated in a sucrose gradient (10–30%) in PBS buffer for 48 h each. Slides were treated with 10 mM citrate buffer at 60°C, permeabilized with PBS-T buffer, and incubated with  $\text{H}_2\text{O}_2$ , followed by incubation with 5% horse serum in PBS buffer for 2 h at 25°C. Then, tissue sections were incubated with anti-mouse Bcl-2 and anti-mouse-Ki67 antibodies (Santa Cruz Biotechnology, Santa Cruz, CA, USA) with a ratio of 1:100 in PBS buffer containing 0.2% horse serum for 24 h at 25°C. The slides were washed three times with PBST buffer, followed by incubation with the secondary antibody (1:500) in PBS [anti-mouse immunoglobulin G (IgG) biotinylated; Vector Labs] for 1 h at 25°C. Antibody reaction was developed using the Vectastain Elite ABC horseradish peroxidase

(HRP) kit (Vector Labs, Inc., Burlingame, CA, USA). In case of frozen tissue, tissue sections of 7  $\mu\text{m}$  were obtained with a cryostat Hyrax C25, Carl Zeiss, Gottingen, Germany, at  $-20^{\circ}\text{C}$ . Images were acquired with a contrast phase inverted-fluorescence microscope (Leica DM 3,000 equipped with a digital CDD, Leica Biosystems Inc., Buffalo Grove, IL, USA). In addition, tumor cells treated with rhodamine 123 (Sigma-Aldrich Co. St. Louis, MO, USA) were observed directly using a confocal microscope (Olympus FV1000, Center Valley, PA, USA); the emission signal of fluorescence was monitored at 533 to 563 nm for rhodamine 123 probe.

## Antibody Array Assay

Melanoma tissue from three to six mice ( $\sim 3\text{g}$ ) were cut into small pieces on ice and homogenized by sonication in 300  $\mu\text{L}$  of phosphorylation buffer (HEPES 50 mM pH 7.6 containing sodium-pyrophosphate 50 mM, sodium orthovanadate 1 mM, sodium molybdate 1 mM, EDTA 20 mM, EGTA 20 mM, benzamidine 1 mM, NaF 20 mM, PMSF 0.2 mM,  $\beta$ -glycerophosphate 80 mM, mannitol 200 mM, and protease inhibitor cocktails 1  $\mu\text{L}/\text{mL}$ ). Then, we used three cycles of sonication at low intensity (20 kHz, 5 W) for 30 s each at  $4^{\circ}\text{C}$  with 5 min of resting between sonication cycles (Hielscher-LS24 Ultrasound Technology, Ringwood, NJ, USA). Cell-free protein extracts were obtained by centrifugation (7,500 g,  $4^{\circ}\text{C}$  for 15 min). Protein concentration was determined using the Bradford reagent (BioRad, Hercules, CA, USA) and 30  $\mu\text{g}$  of total protein were added to each well with glass slides of antibody array kit (PathScan Cancer Phenotype Antibody Array Kit #14,821 and PathScan Intracellular Signaling Array Kit #7,323; Cell Signaling Technology, Danvers, MA, USA). The array glass slides were incubated overnight at  $4^{\circ}\text{C}$  on an orbital shaker. Following immunoreactions and washes, slides were incubated with a biotinylated-antibody cocktail and HRP-linked streptavidin for 1 h at room temperature. To detect immunoreactivity, LumiGlo<sup>®</sup>/Peroxide reagent was added and the image immediately captured using a digital imaging chemiluminescent system, ChemiDoc<sup>™</sup> MP System (BioRad, Hercules, CA, USA). Determination of spot intensity from the microarray was carried out by densitometry analysis using ImageJ software (NIH Image).

## Western Blot Analysis

Proteins from tumor extracts were separated under denaturing conditions using polyacrylamide gel electrophoresis at 10–12% [sodium dodecyl sulfate (SDS)]. Thirty micrograms of protein extracts were typically loaded per lane. Protein mixtures were mixed with 10  $\mu\text{L}$  of denaturing buffer (Tris-HCl 0.06 M, pH 6.8, 5% glycerol, 4% SDS, 4%  $\beta$ -mercaptoethanol, and 0.0025% bromophenol blue) and incubated for 5 min at  $95^{\circ}\text{C}$ . Gels were stained with Coomassie blue and proteins from replicate gels transferred to polyvinylidene difluoride (PVDF; Millipore, Billerica, MA, USA) membranes for immunodetection assays. Briefly, PVDF membranes were incubated with TBS-T (Tris-HCl 10 mM; NaCl 0.9%; tween-20 0.1%, dry milk 5%, pH 7.8). Polyvinylidene difluoride membranes were cut according to range of molecular weight

markers and incubated with the indicated antibodies at the concentration suggested by the manufacturer: anti-CD44, anti-Oct3/4, anti-C-Myc, anti-Ras, anti-SNAIL, anti-MMP-1, anti-E-Cad, anti-vimentin, anti-cytokeratin 1 (CK-1), anti- $\alpha$ -tubulin, anti-Akt (C-20), anti-Akt-phosphorylated 1/2/3 (S-473), anti-mTOR, anti-phosphorylated-mTOR-(S2448), anti- $\beta$ -actin, and anti- $\alpha$ -tubulin (all from Santa Cruz Biotechnology, Santa Cruz, CA, USA) antibodies. Following 12 h of incubation ( $4^{\circ}\text{C}$ ) for the primary antibody, membranes were washed and incubated with goat anti-rabbit IgG HRP-conjugate (1:10,000, BioRad, Hercules, CA, USA), in blocking medium for 4 h at  $4^{\circ}\text{C}$ ; the membranes were washed twice with TBS-T buffer and developed using hydrogen peroxide and Supersignal West Pico Luminol (Pierce; Thermo Fisher Scientific, Waltham, MA, USA). Then images were captured using a ChemiDoc<sup>™</sup> MP System (BioRad, Hercules, CA, USA). Assays were conducted at least three times, and representative images are shown. Band intensities in gel images or films were quantified using the ImageJ software (NIH Image).

## Docking Analysis

Data of the protein structure of mice, rat, and human were obtained from the protein data bank [accession no. AKT (3CQU), HIPK2 (6P5S), AMPK (5UFU), MET (3QTI), JNK (2G01), CD44 (2JCR), and HIF-1 $\alpha$  (5JWP)]. The three-dimensional models of CDPs used in the study were obtained from <https://pubchem.ncbi.nlm.nih.gov/compound/> and as previously described (18). Docking analysis was carried out using the software Autodock 4.2.5.1 (available at <http://autodock.scripps.edu/>). After docking, 100 conformations for each compound were obtained and then clustered for analysis using ADT 1.5.2 software. The conformations selected were within the most represented cluster and corresponded to those showing the lowest values of binding energy and  $K_i$ . Model analyses and figure drawing were carried out with PYMOL 2.1.0 (The PyMOL Molecular Graphics System, version 2.1.0; Schrödinger, LLC, New York, NY, USA; <https://sourceforge.net/p/pymol>).

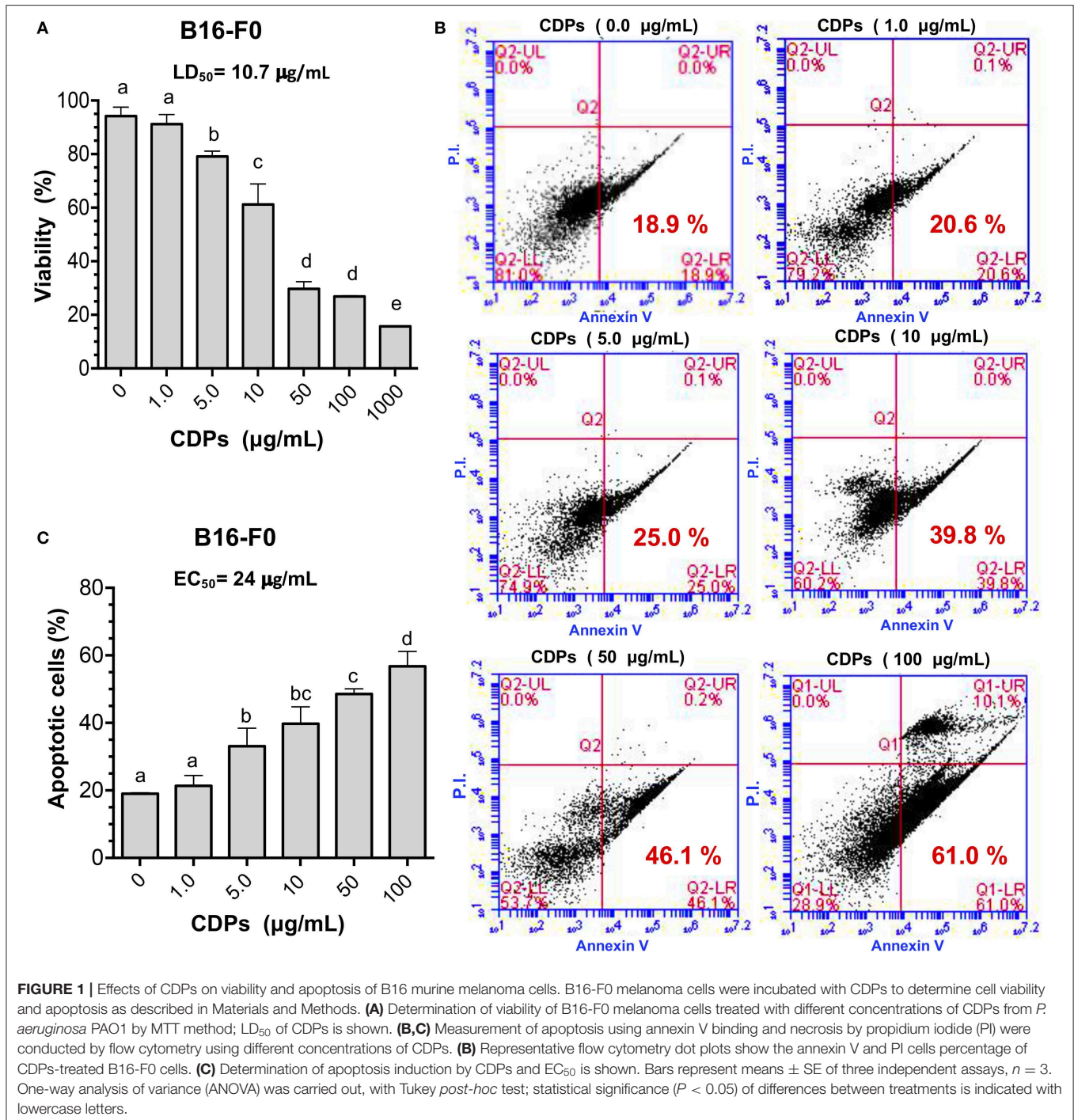
## Statistical Analysis

For correlation analysis, data obtained of antibody arrays and Western blots were analyzed by correlation analysis utilized as response variables (treatments) vs. data of signal intensity for each antibody (cases) using the STATISTICA software (Data Analysis Software System 8.0; Stat Soft Inc., Tulsa, OK, USA). Other data were statistically analyzed using GraphPad Prism 6.0 software (GraphPad Software, San Diego, CA, USA).

## RESULTS

### CDPs From *P. aeruginosa* PAO1 Induce Apoptosis of Murine B16-F0 Melanoma Cells

First, we examined the effect of these compounds on the B16-F0 melanoma line in culture, finding that CDPs decreased viability



of B16-F0 cells in a dose-dependent manner. Cell cultures showed 75% dead cells with CDPs at 50 µg/mL after 12 h, rendering an LD<sub>50</sub> of 10.7 µg/mL (Figure 1A); remarkably, the LD<sub>50</sub> data indicated that CDPs were ~5-fold more bioactive in inducing cell death in the B16-F0 murine melanoma line than in the human HeLa line described previously (6). To further support the CDP effect on the B16-F0 melanoma line, we used annexin V binding to determine apoptotic and PI to determine

necrotic cells by FACS analysis (Figures 1B,C). Whereas, <20% of cells were stained with annexin V in cells incubated with vehicle, ~60% of cells treated with CDPs (50 µg/mL at 4 h) became apoptotic (Figure 1C). The EC<sub>50</sub> of apoptosis induction was ~24 µg/mL at 4 h of treatment (Figure 1B). These data indicated that CDPs from *P. aeruginosa* PAO1 were cytotoxic, inducing apoptosis in the B16-F0 melanoma cell line.

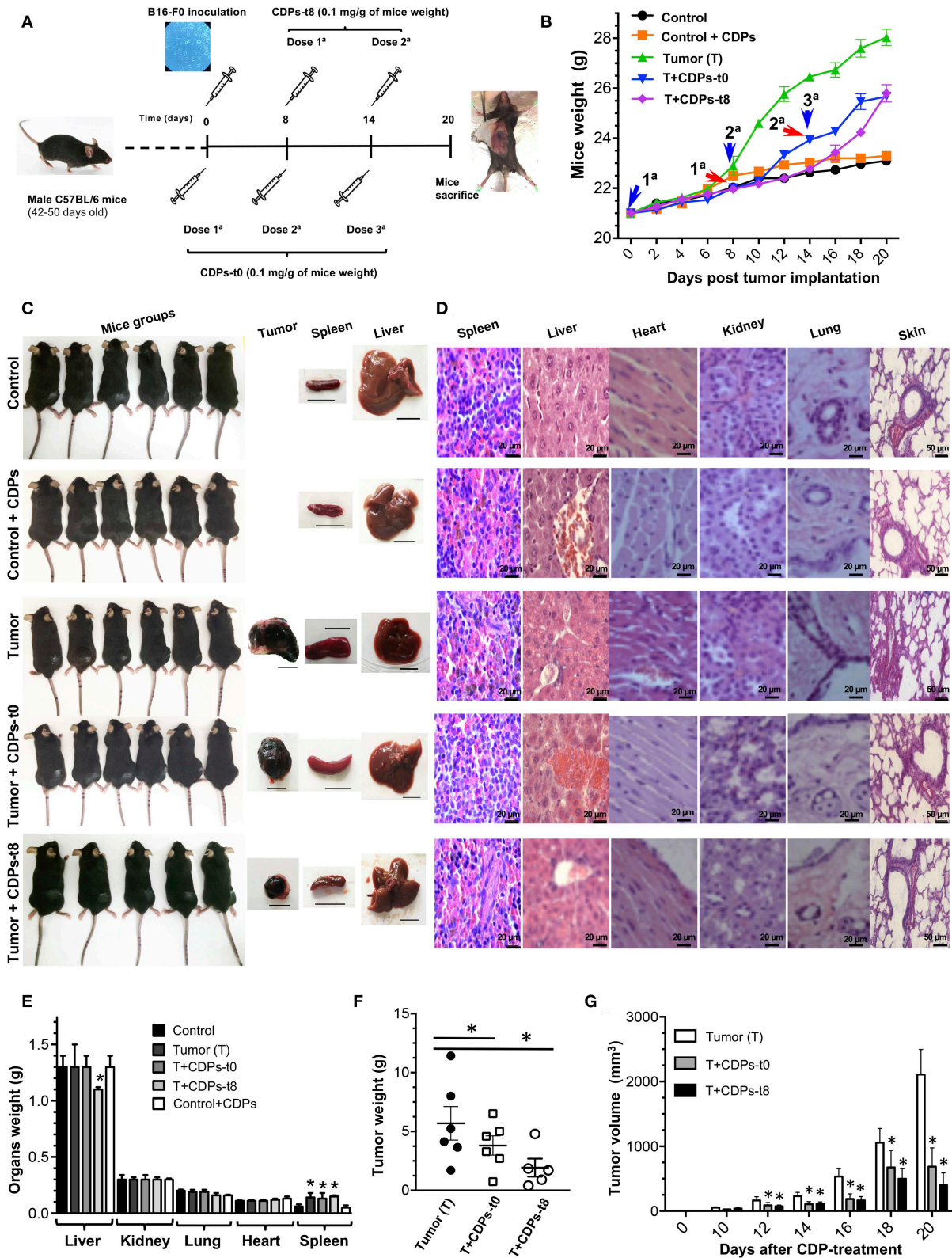


**FIGURE 2 |** Antitumor effect of CDPs on xenografted tumor melanoma B16-F0 cells in mice. **(A)** Experimental design showing tumor implantation and CDP treatments. Mice of 6 weeks of age were weighed, melanoma was implanted subcutaneously, and treatments were started. Mice ( $n = 6$  per group) were treated as *(Continued)*

**FIGURE 2** | indicated. After 20 days, mice were euthanized, organs dissected, and diverse parameters were determined as described in Materials and Methods. **(B)** Determination of mouse weight over 20 days' period. Arrowheads indicate the CDP administration time and dose number. **(C)** Photograph of mouse groups at the 20th day of experimental procedure before euthanizing. Representative photographs of tumor, spleen, and liver from each mouse group are shown. Scale bar was assigned adjusting the scale with the original ruler corresponding to 10 mm. **(D)** Representative hematoxylin-eosin staining of tissue from spleen, liver, heart, kidney, lung, and skin of the mouse groups. Scale bar in  $\mu\text{m}$  is shown. Determination of weight of mouse organs after 20 days **(E)**, tumor weight **(F)**, and tumor volume **(G)**. Bars represent the means  $\pm$  SE of one experiment,  $n = 6$ . One-way ANOVA with Bonferroni *post-hoc* test was used to compare treatments with the untreated group (control) or with tumor group (T); significant differences ( $P < 0.05$ ) are indicated with asterisk (\*).

## Effect of CDPs on Xenografted Melanoma Murine Tumors

To evaluate the antitumorigenic potential of a mixture of bacterial CDPs, we used a subcutaneous xenografted melanoma mouse model (20). Tumors were induced by subcutaneous injection of B16-F0 melanoma cells on male C57BL/6 mice of 10 weeks of age. To determine the effect of CDPs on melanoma development, different mouse groups were tested as described in *Materials and Methods*. Typically, after 8 days, the tumors reached a volume average of 20–50  $\text{mm}^3$ . A group of mice was treated with CDP injection from the beginning of cells implantation (T + CDPs-t0) (**Figure 2A**). Another mouse group was treated after the eighth day of melanoma cells implantation [T + CDPs-t8]. To monitor tumor growth, mice were weighed every 2 days for 20 days (**Figure 2B**). The body weight of mice belonging to the tumor (T) group showed a significant increment in weight. Body weight of mice in both the T + CDPs-t0 and T + CDPs-t8 groups were lower than the T group without CDP treatment, suggesting that the weight increment found in the T group could be related to tumor development. Healthy mice treated with CDPs did not show changes in body weight compared to the control group. All mice survived for 20 days, were humanely euthanized, and tumors and organs removed and weighed (**Figure 2C**). There were no significant differences in weights of kidney, lung, and heart organs; however, a 2-fold increase in the weight and volume of the spleen of the T mouse group was observed (**Figures 2C–E**). A decreased liver weight was also observed in the T + CDPs-t8 group (**Figure 2E**).

Data show that CDP treatment caused a significant decrease in mass and volume of tumors (**Figures 2F,G**). We found that the average weight of the tumors in mice without treatment (T) was  $\sim 5.5$  g, with a tumor volume of  $\sim 2,100$   $\text{mm}^3$ , whereas the tumors from the CDP-treated mouse groups injected immediately with CDPs (T + CDPs-t0), and after the eighth day of melanoma cells implantation [T + CDPs-t8], showed on average  $\sim 4$  and  $\sim 2$  g, with volumes of  $\sim 70$  and  $\sim 30$   $\text{mm}^3$ , respectively, (**Figures 2F,G**). Thus, CDPs decreased size and weight of xenografted tumors formed by B16-F0 melanoma cells in C57BL/6 mice.

Histopathological studies showed no apparent modification of cell size, morphology, and cellular structures from spleen, liver, heart, kidney, lung, and skin in the mice groups (**Figure 2D**). In addition, tissues from the healthy CDP-treated control mouse group were normal; thus, CDP treatments appear to be safe for mice.

Hemoglobin and hematocrit were significantly diminished in the T group (**Figure 3A**). The control mouse group treated with CDPs showed no differences in any of the hematological parameters. Erythrocytes from the T mice group showed

characteristic evidence of echinocytes (frequently found in patients with liver disease; **Figure 3B**). We found that the T mouse group had a reduction in the proportion of lymphocytes accompanied by an increment of neutrophils; these effects were less pronounced in mouse groups treated with CDPs (**Figure 3C**).

We also determined the activity of cell damage marker enzymes LDH, AST, and ALT. The T mouse group showed a significant increment in both LDH and AST enzymatic activities (**Figure 3D**), which were diminished in the tumor-induced mice treated with CDPs (T + CDPs-t0 and T + CDPs-t8). The treatment with CDPs in the healthy CDP-treated control mouse group did not alter LDH and AST levels as shown in the control mouse group. Alanine aminotransferase activity did not show significant differences between the mouse groups, except for the T mouse group. Nevertheless, the ALT/LDH ratio showed significant difference with tumor development and CDP treatment. An increased ALT/LDH ratio ( $\sim 10$ -fold) was observed in the healthy mouse group administered with CDPs (control + CDPs), whereas a lower value of this ratio was observed in the tumor group without CDP treatment (**Figure 3D**).

Histopathological examination showed strong nuclear fragmentation in cells of tumor tissue from mice treated with CDPs (T + CDPs-t0 and T + CDPs-t8); this effect was not observed in the tissues from the untreated (T) mice group (**Figure 3E**). Bcl-2 and Ki67 tumor markers were significantly diminished in the mouse groups that were CDP treated (**Figure 3E**). Additionally, determination of reactive oxygen species (ROS) on cells dissected from tumor tissues using the rhodamine 123 probe was carried out. Confocal microscopic images showed an exacerbated generation of ROS in the cells from tumors of mice treated with CDPs, as well as a loss of cell morphology (**Figure 3E**), indicating an apoptotic and necrotic status on tumor tissues, induced by CDP treatment.

## Cyclodextrins Favor the Antitumor Effect of the CDPs in Xenografted Mouse Melanoma

Because DMSO was the vehicle used to solubilize CDPs, we wondered if the beneficial effect observed on mice with melanoma implantation could be improved by another drug vehicle; we replaced DMSO with a  $\beta$ -cyclodextrin suspension. The CDP-cyclodextrin suspension was administered to the mouse groups with xenografted tumors and compared with treatments where CDPs were dissolved in DMSO. Tumors of the mouse group without treatment (T) showed an average weight of  $\sim 9$  g with a volume of  $\sim 2,200$   $\text{mm}^3$ . The average weight and volume of tumors from mice treated with CDP-dissolved in DMSO were  $\sim 2.5$  g and  $\sim 900$   $\text{mm}^3$ , respectively,

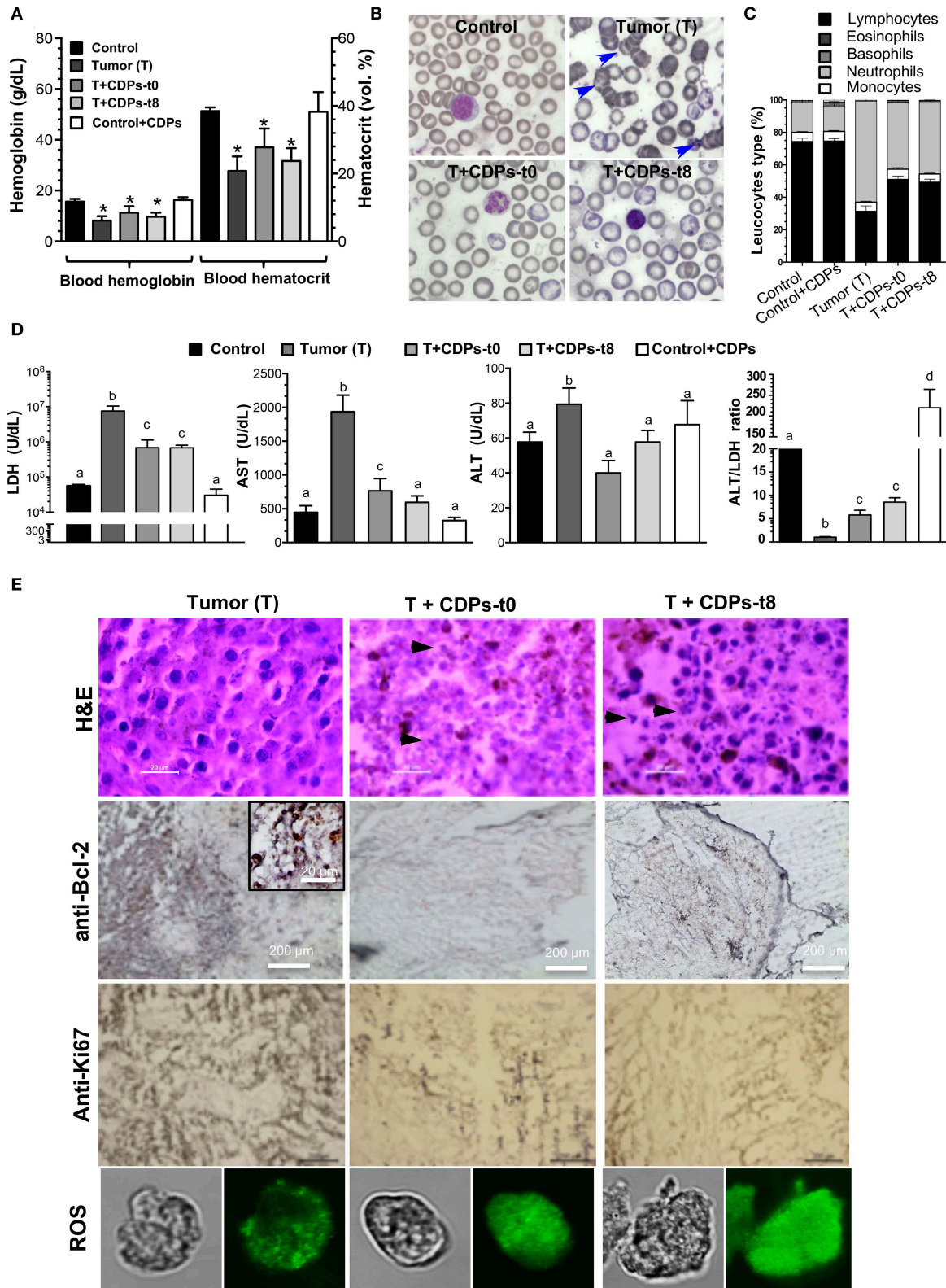


**FIGURE 3 |** Determination of tumor markers in xenografted tumor melanoma mice treated with CDPs. **(A)** Determination of hemoglobin and hematocrit in the blood of the different mouse groups at 20<sup>th</sup> day of experimental procedure before euthanizing. **(B)** Morphology of blood cells (echinocytes are indicated with arrowheads). *(Continued)*

**FIGURE 3 | (C)** Leukocyte differential. **(D)** Determination of lactate dehydrogenase (LDH), aspartate aminotransferase (AST), and alanine aminotransferase (ALT) activities, and the ALT/LDH ratio. Bars represent the means  $\pm$  SE,  $n = 6$ . One-way ANOVA with Bonferroni *post-hoc* test was used to compare treatments with the untreated group (control). Significant differences ( $P < 0.05$ ) are indicated with asterisk (\*) or with lower-case letters. **(E)** Histological analysis of tissue from melanoma tumors by hematoxylin-eosin (H&E) staining, anti-Bcl-2, anti-Ki67 immunoreactivity, and confocal images of tumor cells stained with rhodamine 123 (ROS probe). Scale bar is shown. Arrowheads indicate nucleus fragmentation. Control, healthy mice; control + CDPs, healthy mice treated with CDPs; Tumor (T), mice with tumor implantation without treatment; T + CDPs-t0, mice with tumor implantation and immediately treated after injection; T + CDPs-t8, mice with tumor implantation with CDP treatment at the eighth day of melanoma implantation.

(Figures 4A,C,D). The mouse group treated with the CDP-cyclodextrin suspension administered at the eighth day after melanoma cell injection (T + CDPs-cdxt8) showed an average tumor weight of  $\leq 0.3$  g and a volume of  $\leq 50$  mm<sup>3</sup>; interestingly, in some mice (20%), the tumor was undetectable (Figure 4B). The mouse group treated with CDP-cyclodextrins suspension injected immediately (T + CDPs-cdxt0) showed similar tumor weight with DMSO-CDP treatments, but it showed a significant decrease in tumor volume (Figures 4C,D). Additionally, the cyclodextrins-CDP treatments significantly decreased spleen size and LDH activity compared to those of DMSO-CDPs treated and untreated mouse groups (Figures 4A,E). The lowest LDH activity was observed in the T mouse group treated with CDP-cyclodextrins at the eighth day after tumor implantation (T + CDPs-cdxt8). These results indicate that CDPs were more efficient when they were injected with cyclodextrins suspension compared to DMSO.

## Modulation of Signaling Pathways by CDPs Treatment in Xenografted Mouse Melanoma

To identify elements dysregulated in cancer and possible cell-signaling pathways targeted by the antitumorigenic effect of the CDPs in the xenografted melanoma mouse model, protein extracts obtained from tumor tissue were used for an immunodetection approach. Results of the cancer and signaling antibody arrays showed that tumors presented a significant increase in the expression of proliferative cell nuclear antigen (PCNA), p27Kip1, N-cadherin, HIF-1 $\alpha$ , Stat-3, Akt-S473, AMPka, mTOR-S2448, HSP27, Bad, PRAS40, SAPK/JNK, and caspase-3 (Figures 5A–C), which were significantly recovered/diminished in their expression/phosphorylation level by CDP treatment. Additionally, in the T + CDPs mouse group, CDPs caused an increment in the expression of elements such as survivin, Met, and EGF (Figures 5A–C).

Because we observed an increment in expression of signaling pathways such as PI3k/Akt/mTOR expression in tumors and its recovery level of expression after CDP-treatment, we looked at the activation of Akt-S473, mTOR-S2448, S6k-T389, and other members of signaling pathways such as Xiap, PDK1, NF $\kappa$ B p65, and TNF- $\alpha$ /FasL (Figure 6A). Phosphorylation of Akt-S473 and S6k-T389 was strongly activated in the tumor mouse group (T), whereas a decrease was observed with CDP treatment, but no difference in activation was observed for mTOR-S2448 (Figure 6A). In contrast, Xiap, PDK1, NF $\kappa$ B p65, and TNF- $\alpha$ /FasL did not show significant differences in expression level

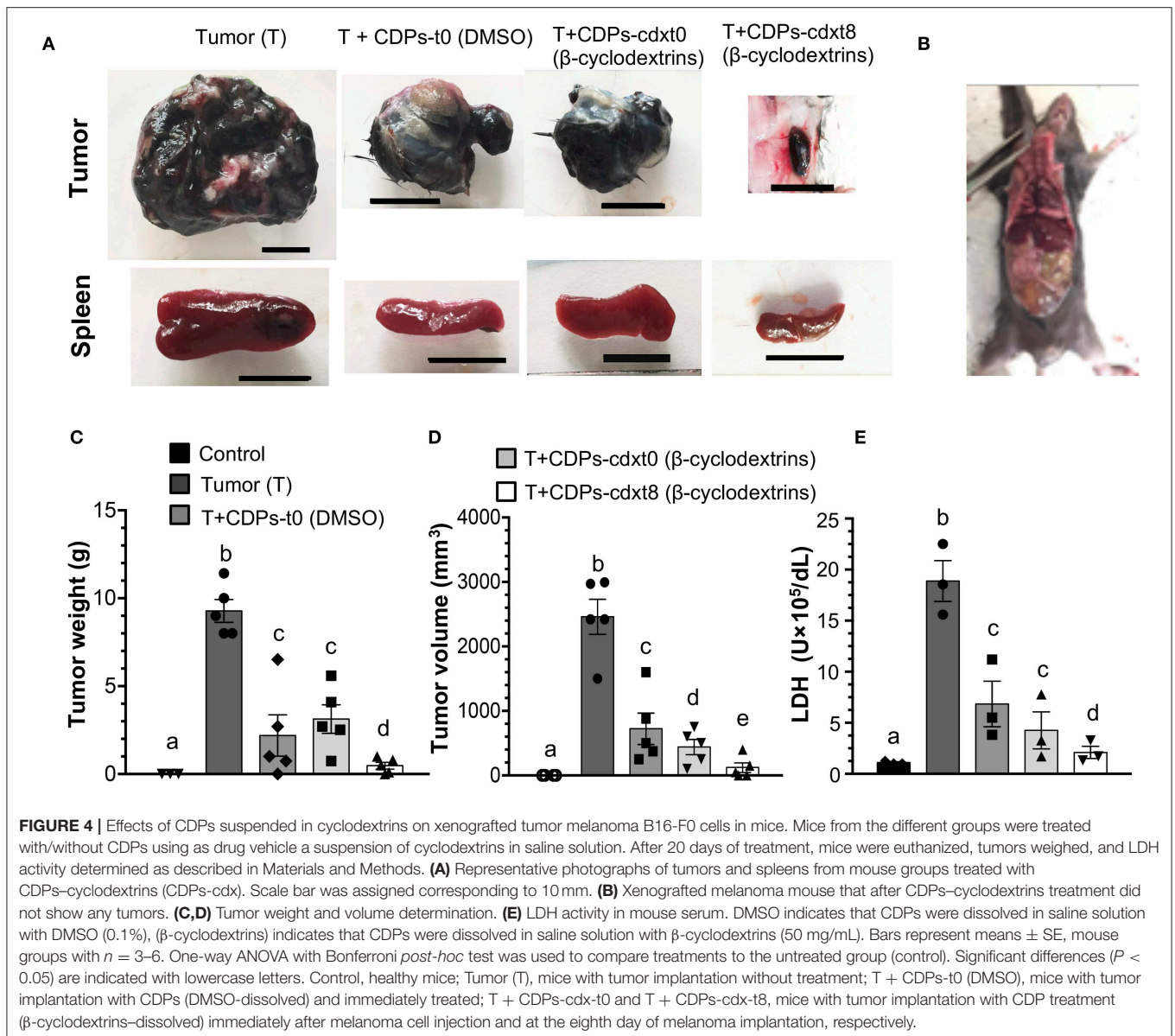
in the CDP-treated mouse group with respect to the T group (Figure 6A).

We also looked at markers of malignancy (i.e., cancer stem cells, pluripotency, and metastasis). Figure 6B shows that the expression of stem cell marker CD44 was decreased to  $<30\%$  in protein extracts of tumors from T + CDPs-t0 mouse group and was totally depressed in the T + CDPs-t8 group; in contrast, the Oct3/4 showed low expression levels in the T mice group, with expression levels increased in the T + CDPs-t8 group. With respect to the oncogenes, c-Myc was decreased, but Ras was increased in the T + CDPs mouse group. Furthermore, the expression of EMT markers such as SNAIL increased in tumors and CDP-treated tumors. However, MMP-1, E-cadherin, vimentin, and CK-1 showed a significantly decreased expression in tumors treated with CDPs (Figure 6B). These results clearly indicate that, in addition to the PI3k/Akt/mTOR pathway, other signaling pathways are involved in melanoma development as in B16-F0 cells line as in tumor of xenografted melanoma cells, and these also may be targeted by the bacterial CDPs.

## DISCUSSION

The quest for novel molecules to target cancer has led investigations to look at microbial metabolites. Cyclic peptides constitute a diverse family of molecules mainly of microbial origin that have antimicrobial, immunomodulator, antioxidant, or anticancerigenic activities (7, 21). Recently, CDPs have attracted attention because of their antiproliferative effects on cancer cell lines (3–6, 22). We recently reported that a mixture of CDPs composed of cyclo(L-Pro-L-Tyr), cyclo(L-Pro-L-Val), and cyclo(L-Pro-L-Phe) isolated from *P. aeruginosa* PAO1 culture inhibited the proliferation of HeLa and CaCo-2 cells (4). In addition, we found that bacterial CDPs are stronger antiproliferative agents compared to chemically synthesized analogs (6). Thus, it appears that CDPs from biological sources are more potent than synthetic CDPs due probably to structural differences in stereospecificity.

Cyclodipeptides affected the viability of B16-F0 cells by inducing apoptosis in cultured cells (Figure 1). Although CDP's biological properties have been studied *in vitro*, we now show that CDPs can inhibit melanoma tumor progression in mice. Interestingly, we showed that mice implanted with B16-F0 cells and simultaneously treated with CDPs did not develop tumors, unlike untreated mice. Importantly, in tumors already developed, tumor size was decreased in mice treated with CDPs (Figures 2–4). Mice that developed tumors showed diminished blood cell counts, which correlated with an increment in spleen size (Figures 2, 3), symptoms that are indicative of an anemic



status seen in patients with cancer (23). Cyclodipeptide treatment of the tumor-induced mice resulted in a recovery of hematologic parameters (Figures 3A–C). Furthermore, LDH, ALT, and AST increased in mice with tumors as described in liver and breast cancers (24, 25), but the levels of these enzymes significantly decreased when mice were treated with CDPs (Figure 3D). Interestingly, the control mouse group treated with CDPs did not show altered values of these blood and enzymes levels, suggesting that, at least, the injected amount of CDPs was not toxic to mice. Levels of LDH, ALT, and AST are used as markers of disease evolution of anticancer treatments (25). We observed a recovery of the levels of LDH and AST in mice treated with CDPs similar to those found in healthy mice (Figure 3D). This was not observed in the untreated group. These results indicate an improvement in health of mice bearing tumors treated

with CDPs. In addition, histological and immunohistochemical data showed strong nuclear fragmentation and decreased Bcl-2 and Ki67 cancer marker levels in tumor tissues from mice treated with CDPs (Figure 3E). Images of tissue showed an exacerbated generation of ROS in tumors from CDP-treated mice, confirming the induction of apoptosis, dependent on mitochondrial dysfunction and cytochrome *c* release.

An important issue to consider in therapeutic treatments is the drug bioavailability; in this sense, we improved the bioavailability of the CDPs using a suspension in β-cyclodextrins. Results obtained in our xenografted melanoma mouse model showed that the CDPs dissolved in cyclodextrins were more efficient in inhibiting tumorigenesis than those dissolved in DMSO (Figure 4), suggesting that the antitumorigenic effect of the CDPs could be improved by utilization of an appropriate drug vehicle.

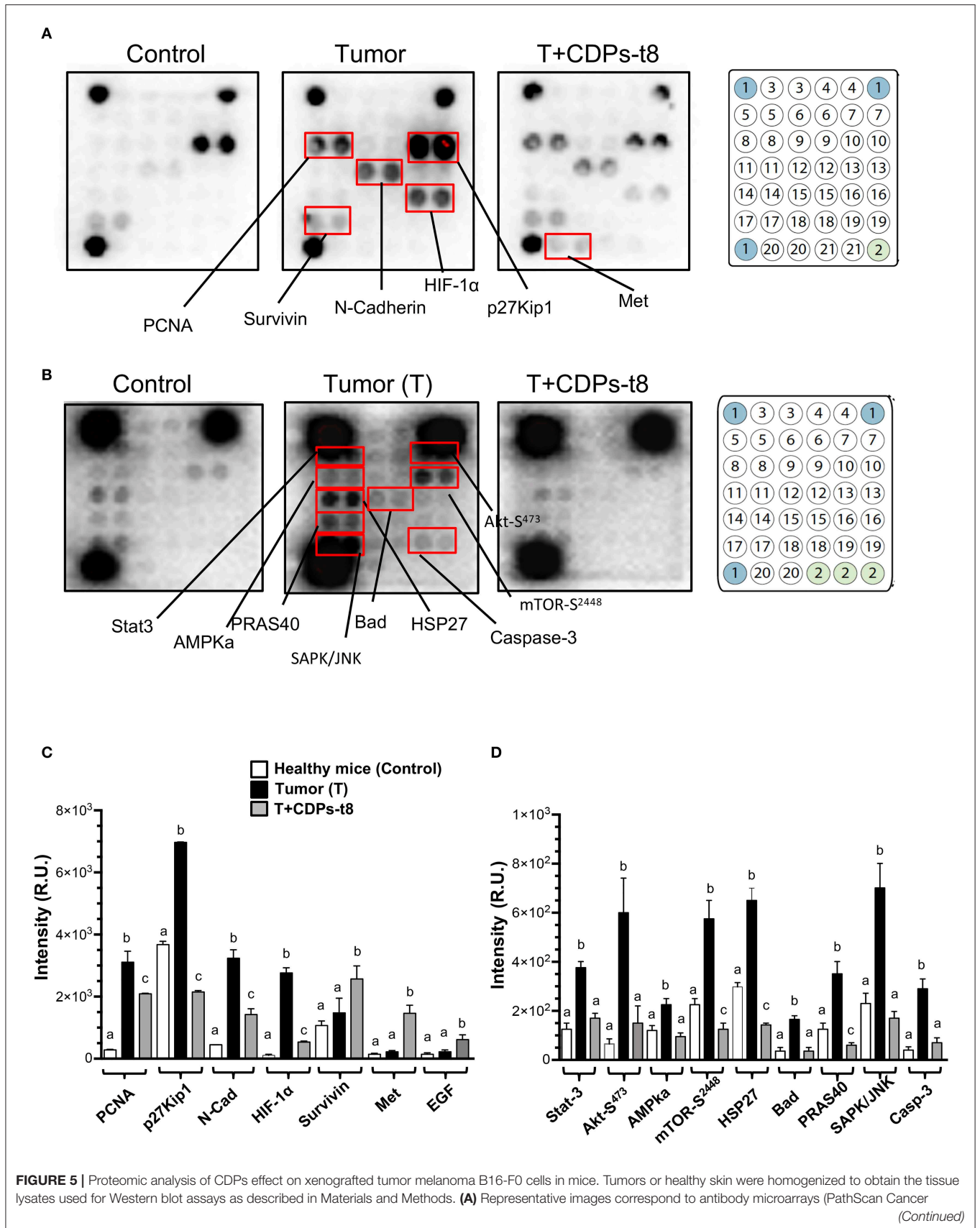


**FIGURE 5 |** Phenotype Antibody Array. The arrays contained the following antibodies: (1) positive control, (2) negative control, (3) CD31, (4) EpCAM, (5) vimentin, (6) CD44, (7) CD45, (8) PCNA, (9) Ki-67, (10) p27Kip1, (11) E-cadherin, (12) N-cadherin, (13) VE-cadherin, (14) MUC1, (15) Rb Ser807/811, (16) HIF-1 $\alpha$ , (17) survivin, (18) P53, (19) HER2/ErbB2, (20) Met, (21) EGF. **(B)** Representative images correspond to antibody micro-arrays (PathScan Intracellular Signaling Array). The arrays contained the following antibodies: (1) positive control, (2) negative control, (3) ERK1/2-Thr202/Tyr204, (4) Stat1-Tyr701, (5) Stat3-Tyr705, (6) Akt-Thr308, (7) Akt-Ser473, (8) AMPK $\alpha$ -Thr172, (9) S6 Ribosomal Protein-Ser235/236, (10) mTOR-Ser2448, (11) HSP27-Ser78, (12) Bad-Ser112, (13) p70S6 Kinase-Thr389, (14) PRAS40-Thr246, (15) p53-Ser15, (16) p38-Thr180/Tyr182, (17) SAPK/JNK-Thr183/Tyr185, (18) PARP-Asp214, (19) caspase-3-Asp175, (20) GSK-3 $\beta$ -Ser9. Proteins that showed differences in expression/phosphorylation levels compared to the control protein extract are indicated. **(C,D)** Determination of signal intensity of spots from microarrays **(A,B)**, respectively, was conducted by densitometry using ImageJ software (NIH). Data represent the means  $\pm$  SE of at two independent assays with spot duplication for each antibody, using protein extracts obtained from at least three tumors of each mouse group. Bars represent means  $\pm$  SE of four densitometry determinations. One-way ANOVA was carried out, with Bonferroni *post-hoc* test; statistical significance ( $P < 0.05$ ) of differences between treatments is indicated with lowercase letters. Control, healthy mice; Tumor (T), mice with tumor implantation without treatment; T + CDPs-t8, mice with tumor implantation treated with CDPs at the eighth day of melanoma implantation.

To determine the molecular mechanism involved in the antitumorigenic effect of CDPs in the xenografted melanoma mouse model, we utilized antibody arrays to screen in tumors, differential expression of proteomic elements related to cancer disease, and intracellular signaling pathways (**Figure 5**). Previously, we found that the CDP mixture from *P. aeruginosa* PAO1 was able to repress phosphorylation of both Akt-S473 and S6k-T-389 protein kinases in HeLa cells at short treatment times (6). The PI3K/Akt/mTOR pathway is up-regulated in more than 70% of cancer types (26, 27). In our murine melanoma model, we also found up-regulation of PI3k/Akt/mTOR pathway (**Figure 6**). In this study, also hyperactivation of phosphorylation in melanoma tumors from mice was found, where the level of phosphorylation was decreased in tumors from CDP-treated mice. Thus, it further confirms that CDPs targeted the mTOR pathway, which is critical for cell growth and proliferation. Apoptosis dependent on the Akt-Ser473 inhibition and downstream target proteins by CDPs in our melanoma model indicates the participation of the mTORC1 and mTORC2 complexes in blocking the PI3K/Akt/mTOR signaling pathway; in agree with recent findings described in HeLa cells (28). In agreement with these results, dual inhibition of the mTORC1 and mTORC2 signaling pathways has been proposed as effective therapeutic targets in neoplasias (29, 30). It suggests that CDPs can be considered as potential therapeutic compounds in melanoma by causing dual inhibition of mTORC1 and mTORC2 complexes.

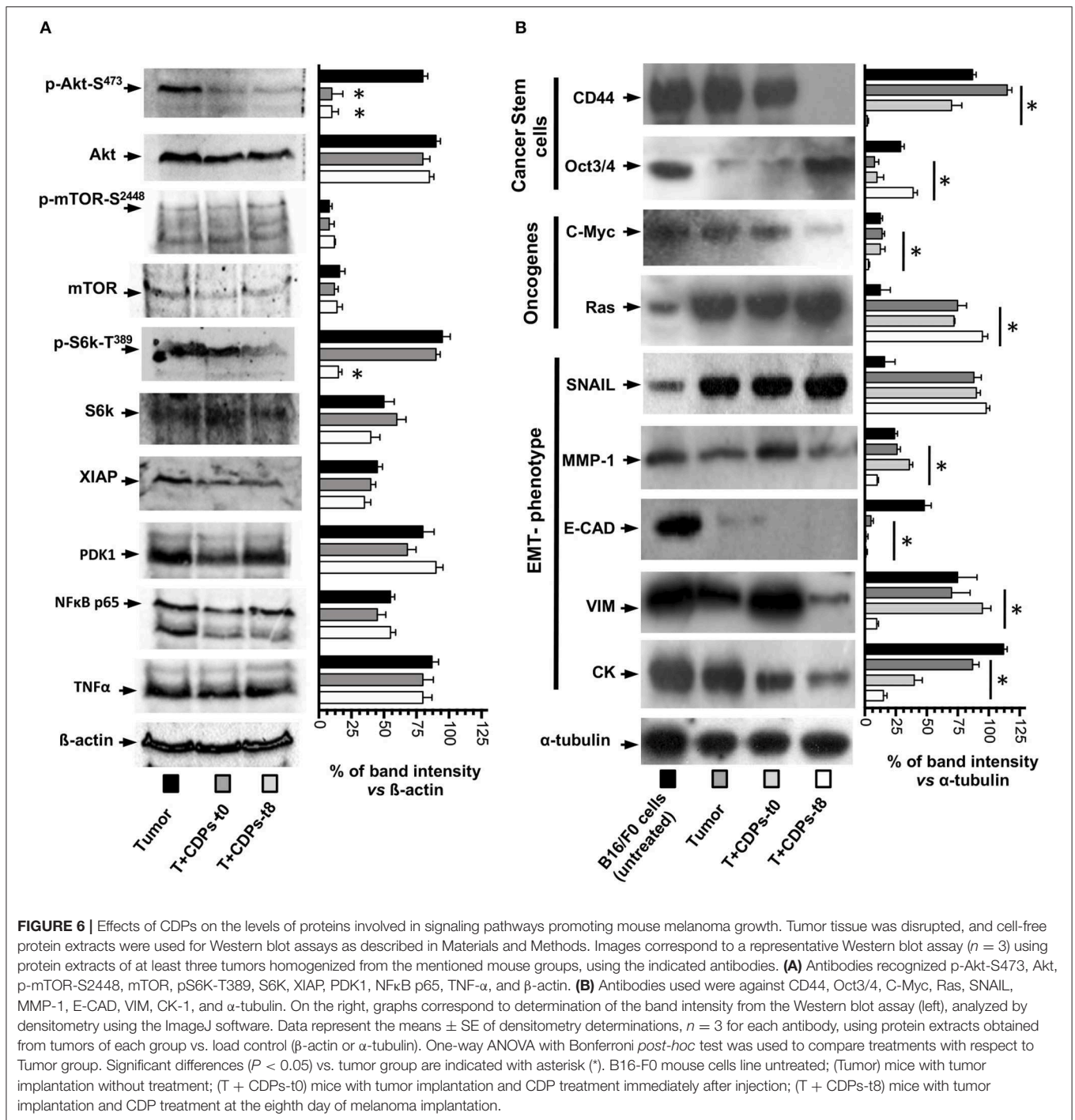
Additionally, we observed an up-regulation of HIF-1 $\alpha$  protein in tumors of xenografted melanoma mice (**Figure 5**). The HIF-1 suppressor is a master regulator of elements involved in glycolysis and is dysregulated in tumorigenesis and invasiveness. It is well-known that the regulation of HIF-1 is closely related to the PI3K/Akt/mTOR pathway. Functionally, it has been shown that Akt and HIF-1 interact synergistically during the development of melanoma (31). Our data show that the PI3K/Akt/mTOR and HIF-1 cross-talk pathways are implicated in mouse melanoma development and that CDPs targeted these pathways. Because HIF-1 regulates processes such as survival, apoptosis, glucose metabolism, angiogenesis, and invasiveness by inducing EMT regulators (32–34), it is attractive to postulate that the antitumor effects of CDPs may be mediated by affecting HIF-1 and reflected in the blocking of cell invasion. In addition, the PCNA, which acts during the S and G2 phases of the cell cycle, is considered a marker of cell proliferation, which actively participates

in a number of signaling pathways responsible for cell survival (35).

We found that the transcription factor SNAIL is up-regulated in melanoma tumors, whereas expression of CD44 and E-Cad is down-regulated (**Figure 6B**). SNAIL is a prominent inducer of EMT and strongly represses E-cadherin expression. Cyclodipeptides increased SNAIL levels and decreased levels of the hyaluronan receptor CD44, a cell surface adhesion receptor that is highly expressed in many cancers and regulates metastasis by alternative splicing and recruitment of CD44 to the cell surface (36).

Furthermore, important tumorigenic markers were repressed in the CDP-treated mice, such as C-Myc, MMP-1, E-cadherin, vimentin, and CK-1 (**Figure 6B**). These data support the hypothesis that CDPs may promote the activation/repression of the main components of the EMT pathway to induce apoptosis in tumors and probably inhibit tumorigenesis and invasiveness. On the other hand, Xiap, PDK1, NF $\kappa$ B p65, and TNF- $\alpha$ /FasL did not show significant differences in their expression level in the CDP-treated mouse group with respect to the T group (**Figure 6A**), suggesting that these elements play important roles in signaling pathways in which their participation is not affected by the CDPs; however, this does not rule out their involvement.

An approach analysis of the multiple factors and pathways evaluated in our melanoma tumorigenesis model with treatment with bacterial CDPs was conducted using a statistical correspondence analysis (**Figure 7A**). Data show that the cancer factors clearly correlated in up-expressed/activated and down-expressed/inactivated as widely described (**Figure 7A**). An important number of proteins are associated with the response variable (control), which were not modified in their expression level in tumors CDPs-treated and untreated groups. A second group of proteins that showed significant changes in their expression levels in the proteomic approach was associated with the response variable Tumor mouse group which developed tumors without treatment. This group of proteins corresponds to oncogenes and tumor suppressors widely associated with tumorigenesis. Finally, a third group of proteins highly implicated in the control of tumorigenesis, invasiveness, and signaling pathways such as PI3K/Akt/mTOR, Ras/ERK, EMT, CSC, and so on, was associated with the CDPs-treated mouse group (**Figure 7A**). From this correlation analysis, some representative proteins of each group were selected and



analyzed by molecular docking using the crystallographic structures with ligands, such as substrate or inhibitors, and evaluated for the feasibility of interaction with the CDPs as modulator molecules (Figure 7B). Docking approach showed that the CDPs may interact with protein kinase members of multiple signaling pathways. The cyclo(L-Pro-L-Tyr) and cyclo(L-Pro-L-Phe) showed better predicted interaction values ( $K_i$  of 2–65  $\mu$ M and binding energy of  $-7.8$  to  $-7$  kCal/mol),

than cyclo(L-Pro-L-Val) (Table S1). Docking revealed that the CDPs have the potential to interact in different sites of protein kinases such as substrate-binding site, inhibitor-binding site or co-substrate-binding site. Analysis also predicted a differential affinity for the CDPs, being cyclo(L-Pro-L-Tyr) in general the most potent as inhibitor. Structural images of proteins kinases AKT, HIPK2, AMPK, MET, JNK, HIF-1 $\alpha$ , and CD44 with the interaction with the cyclo(L-Pro-Tyr) are shown in Figure 7B.

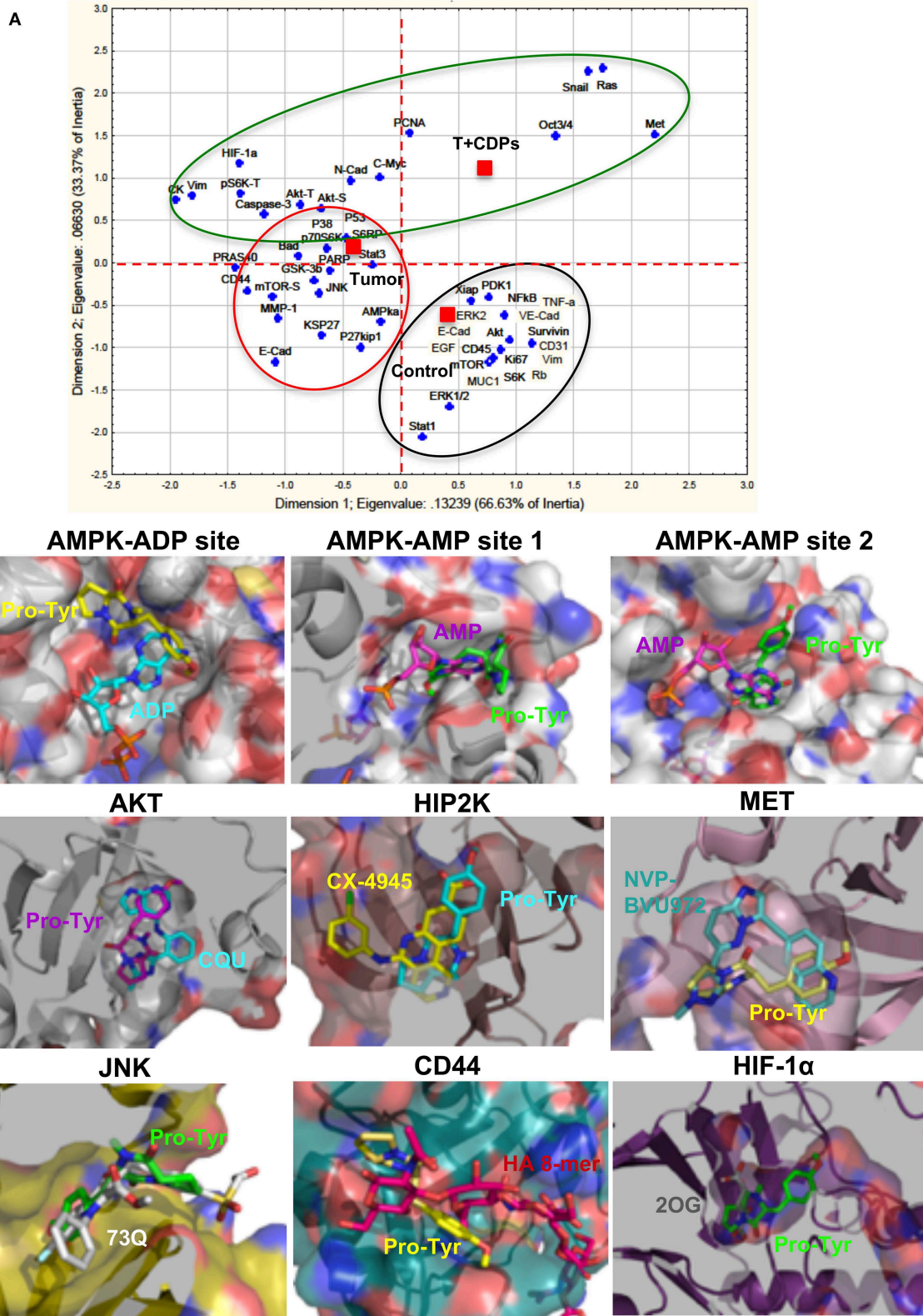


**FIGURE 7 |** Correlation analysis of proteomic approach on xenografted tumor melanoma B16-F0 cells in mice treated with CDPs and docking analysis. **(A)** Correlation analysis of densitometry data from microarrays and Western blots (**Figures 5, 6**) were analyzed by multivariate exploratory techniques, using the *(Continued)*

**FIGURE 7** | correspondence analysis (CA) of the STATISTICA Software System 8.0 (Stat Soft Inc., Tulsa, OK, USA). Correlation groups are as follows: healthy mice (control); mice with tumor implantation without treatment (Tumor); mice with tumor implantation and CDP treatment (T + CDPs). **(B)** Docking analysis of the CDP cyclo(L-Pro-L-Tyr) in the binding sites of tyrosine-kinases. A slice of the protein showing the catalytic or inhibitor binding sites of protein kinases is presented with the orientation of the CDP (Pro-Tyr) in the predicted conformations. The protein is shown as surface with the interior in cartoon; Pro-Tyr and other molecules are shown as sticks colored by elements. Pro-Tyr, cyclo(L-Pro-L-Tyr); CQU, (N-[2-(5-methyl-4H-1,2,4-triazol-3-yl)phenyl]-7H-pyrrolo[2,3-d]pyrimidin-4-amine); CX-4945, 5-[(3-chlorophenyl)amino]benzo[c][2,6]naphthridine-8-carboxylic acid; NVP-BVU972, 6-[[6-(1-methylpyrazol-4-yl)imidazo[1,2-b]pyridazin-3-yl]methyl]quinolone; 73Q, 6-chloro-9-hydroxy-1,3-dimethyl-1,9-dihydro-4H-pyrazolo[3,4-B]quinolin-4-one; HA 8-mer, hyaluronan octamer; 2OG, 2-oxoglutarate. Models were carried out with PYMOL 2.1.0 (The PyMOL Molecular Graphics System, version 2.1.0; Schrödinger, LLC, New York, NY, USA).

In agreement with our results, some reports have described that some melanoma treatments implicate the use of tyrosine kinase inhibitors such as the MAPK pathway, PI3K (16). Thus, we can propose that inhibition or activation of the protein kinases such as AKT, HIPK2, AMPK, MET, JNK, HIF-1 $\alpha$ , and CD44 by treatment with CDPs in the mouse melanoma model could involve the blocking of the substrate binding site as a molecular mechanism.

Melanoma tumors in mouse showed a significant decrease in factors involved in survival, proliferation, invasiveness, angiogenesis, and glucose metabolism. Thus, our data suggest that bacterial CDPs suppress the activation of the signaling pathways associated with the onset of tumorigenesis governed by PI3K/Akt/mTOR, Ras-ERK, PI3K/JNK/PKA, p27Kip1/CDK1/survivin, MAPK, HIF-1, EMT, and CSC not actually shown. Although the mode of action of CDPs is not totally elucidated, we propose that CDPs target multiple pathways and processes (oncogenes and tumor suppressors) involved in tumor formation and progression by blocking the catalytic site conserved in the serine-threonine kinase family. Findings indicate that the multiple signaling pathways are implicated in melanoma aggressiveness, showing that bacterial CDPs interfere during melanoma development by a mechanism dependent on protein kinase inhibition. Our data suggest that CDPs have potential antiproliferative properties to be used as antineoplastic drugs.

## DATA AVAILABILITY STATEMENT

All datasets generated for this study are included in the article/**Supplementary Material**.

## ETHICS STATEMENT

The animal study was reviewed and approved by the Institutional Committee for Use of Animals of the Universidad Michoacana

## REFERENCES

- Fischbach MA, Segre JA. Signaling in host-associated microbial communities. *Cell*. (2016) 164:1288–300. doi: 10.1016/j.cell.2016.02.037
- Martinez KB, Leone V, Chang EB. Microbial metabolites in health and disease: navigating the unknown in search of function. *J Biol Chem*. (2017) 292:8553–9. doi: 10.1074/jbc.R116.752899
- Nishanth Kumar S, Dileep C, Mohandas C, Nambisan B, Ca J. Cyclo(D-Tyr-D-Phe): a new antibacterial, anticancer, and antioxidant cyclic dipeptide from *Bacillus sp.* N strain associated with a rhabditid entomopathogenic nematode. *J Pept Sci*. (2014) 20:173–85. doi: 10.1002/psc.2594
- Vázquez-Rivera D, González O, Guzmán-Rodríguez J, Díaz-Pérez AL, Ochoa-Zarzosa A, López-Bucio J, et al. Cytotoxicity of cyclodipeptides from *Pseudomonas aeruginosa* PAO1 leads to apoptosis in human cancer cell lines. *Biomed Res Int*. (2015) 2015:197608. doi: 10.1155/2015/197608
- Brauns SC, Milne P, Naude R, Van de Venter M. Selected cyclic dipeptides inhibit cancer cell growth and induce apoptosis in HT-29 colon cancer cells. *Anticancer Res*. (2004) 24:1713–9.

de San Nicolás de Hidalgo. The study was carried out in accordance with the Mexican Official Regulations for the Use and Care of Animals (NOM 062-ZOO- 1999, Ministry of Agriculture, Mexico).

## AUTHOR CONTRIBUTIONS

JC-G: conception and design. MD-M, LH-P, JG-P, AD-P, and LM-A: development of methodology. JC-G, JR-Z, GP-R, and JM: analysis and interpretation of data. JC-G, JR-Z, HR, GP-R, and JM: writing, review, and/or revision of the manuscript. JC-G, JR-Z, and HR: administrative, technical, or material support. JC-G, JR-Z, and GP-R: study supervision. All authors read and approved the final manuscript.

## FUNDING

This study was funded by the Consejo Nacional de Ciencia y Tecnología (CONACYT) of México (Grant Nos. 256119 and 222405) and the Marcos Moshinsky Foundation and Universidad Michoacana de San Nicolás de Hidalgo/C.I.C.2.14 grants. MD-M and LH-P received a scholarship from CONACYT. GP-R and JM were supported by the Intramural Research Program [National Institutes of Health (NIH), National Heart, Lung, and Blood Institute (NHLBI)].

## ACKNOWLEDGMENTS

We thank R. Noriega for the B16-F0 murine melanoma line and Madeline Hernandez for care of animals of the intramural research program.

## SUPPLEMENTARY MATERIAL

The Supplementary Material for this article can be found online at: <https://www.frontiersin.org/articles/10.3389/fonc.2020.01111/full#supplementary-material>

6. Hernandez-Padilla L, Vazquez-Rivera D, Sanchez-Briones LA, Diaz-Perez AL, Moreno-Rodriguez J, Moreno-Eutimio MA, et al. The antiproliferative effect of cyclodipeptides from *Pseudomonas aeruginosa* PAO1 on HeLa cells involves inhibition of phosphorylation of Akt and S6k kinases. *Molecules*. (2017) 22:1024. doi: 10.3390/molecules22061024
7. Boyer N, Morrison KC, Kim J, Hergenrother PJ, Movassaghi M. Synthesis and anticancer activity of epipolythiodiketopiperazine alkaloids. *Chem Sci*. (2013) 4:1646–57. doi: 10.1039/c3sc50174d
8. Borders EB, Bivona C, Medina PJ. Mammalian target of rapamycin: biological function and target for novel anticancer agents. *Am J Health Syst Pharm*. (2010) 67:2095–106. doi: 10.2146/ajhp100020
9. Laplante M, Sabatini DM. mTOR signaling in growth control and disease. *Cell*. (2012) 149:274–93. doi: 10.1016/j.cell.2012.03.017
10. Kim YC, Guan KL. mTOR: a pharmacologic target for autophagy regulation. *J Clin Invest*. (2015) 125:25–32. doi: 10.1172/JCI73939
11. Allen-Petersen BL, Risom T, Feng Z, Wang Z, Jenny ZP, Thoma MC, et al. Activation of PP2A and inhibition of mTOR synergistically reduce MYC signaling and decrease tumor growth in pancreatic ductal adenocarcinoma. *Cancer Res*. (2019) 79:209. doi: 10.1158/0008-5472.CAN-18-0717
12. Hanahan D, Weinberg RA. The hallmarks of cancer. *Cell*. (2000) 100:57–70. doi: 10.1016/S0092-8674(00)81683-9
13. Mariotti A, Perotti A, Sessa C, Ruegg C. N-cadherin as a therapeutic target in cancer. *Expert Opin Investig Drugs*. (2007) 16:451–65. doi: 10.1517/13543784.16.4.451
14. Klezovitch O, Vasioukhin V. Cadherin signaling: keeping cells in touch. *F1000Research*. (2015) 4:550. doi: 10.12688/f1000research.6445.1
15. Domingues B, Lopes JM, Soares P, Pópulo H. Melanoma treatment in review. *Immunotargets Ther*. (2018) 7:35–49. doi: 10.2147/ITT.S134842
16. Leonardi GC, Falzone L, Salemi R, Zanghi A, Spandidos DA, McCubrey JA, et al. Cutaneous melanoma: from pathogenesis to therapy (review). *Int J Oncol*. (2018) 52:1071–80. doi: 10.3892/ijo.2018.4287
17. Ortiz-Castro R, Diaz-Pérez C, Martínez-Trujillo M, del Río RE, Campos-García J, López-Bucio J. Transkingdom signaling based on bacterial cyclodipeptides with auxin activity in plants. *Proc Natl Acad Sci USA*. (2011) 108:7253–8. doi: 10.1073/pnas.1006740108
18. Gonzalez O, Ortiz-Castro R, Diaz-Perez C, Diaz-Perez AL, Magana-Duenas V, Lopez-Bucio J, et al. Non-ribosomal peptide synthases from *Pseudomonas aeruginosa* play a role in cyclodipeptide biosynthesis, quorum-sensing regulation, and root development in a plant host. *Microb Ecol*. (2017) 73:616–29. doi: 10.1007/s00248-016-0896-4
19. Sharma S, Stolina M, Lin Y, Gardner B, Miller PW, Kronenberg M, et al. T Cell-derived IL-10 promotes lung cancer growth by suppressing both T cell and APC function. *J Immunol*. (1999) 163:5020–8.
20. Overwijk WW, Restifo NP. B16 as a mouse model for human melanoma. *Curr Protoc Immunol*. (2001) Chapter 20:Unit 20.21. doi: 10.1002/0471142735.im2001s39
21. Borthwick AD. 2,5-Diketopiperazines: synthesis, reactions, medicinal chemistry, and bioactive natural products. *Chem Rev*. (2012) 112:3641–716. doi: 10.1021/cr200398y
22. Furukawa T, Akutagawa T, Funatani H, Uchida T, Hotta Y, Niwa M, et al. Cyclic dipeptides exhibit potency for scavenging radicals. *Bioorg Med Chem*. (2012) 20:2002–9. doi: 10.1016/j.bmc.2012.01.050
23. Hung N, Shen CC, Hu YW, Hu LY, Yeh CM, Teng CJ, et al. Risk of cancer in patients with iron deficiency anemia: a nationwide population-based study. *PLoS ONE*. (2015) 10:e0119647. doi: 10.1371/journal.pone.0119647
24. Thornburg JM, Nelson K, Clem BF, Lane AN, Arumugam S, Simmons A, et al. Targeting aspartate aminotransferase in breast cancer. *Breast Cancer Res*. (2008) 10:R84. doi: 10.1186/bcr2154
25. Cao R, Wang LP. Serological diagnosis of liver metastasis in patients with breast cancer. *Cancer Biol Med*. (2012) 9:57–62. doi: 10.3969/j.issn.2095-3941.2012.01.011
26. Karbowiczek M, Spittle CS, Morrison T, Wu H, Henske EP. mTOR is activated in the majority of malignant melanomas. *J Invest Dermatol*. (2008) 128:980–7. doi: 10.1038/sj.jid.5701074
27. Song M, Bode AM, Dong Z, Lee MH. AKT as a therapeutic target for cancer. *Cancer Res*. (2019) 79:1019–31. doi: 10.1158/0008-5472.CAN-18-2738
28. Hernández-Padilla L, Reyes de la Cruz H, Campos-García, J. Antiproliferative effect of bacterial cyclodipeptides in the HeLa line of human cervical cancer reveals multiple protein kinase targeting, including mTORC1/C2 complex inhibition in a TSC1/2-dependent manner. *Apoptosis*. (2020). doi: 10.1007/s10495-020-01619-z. [Epub ahead of print].
29. Chresta CM, Davies BR, Hickson I, Harding T, Cosulich S, Critchlow SE, et al. AZD8055 is a potent, selective, and orally bioavailable ATP-competitive mammalian target of rapamycin kinase inhibitor with *in vitro* and *in vivo* antitumor activity. *Cancer Res*. (2010) 70:288–98. doi: 10.1158/0008-5472.CAN-09-1751
30. Kawata T, Tada K, Kobayashi M, Sakamoto T, Takiuchi Y, Iwai F, et al. Dual inhibition of the mTORC1 and mTORC2 signaling pathways is a promising therapeutic target for adult T-cell leukemia. *Cancer Sci*. (2018) 109:103–11. doi: 10.1111/cas.13431
31. Sanchez-Hernandez I, Baquero P, Calleros L, Chiloeches A. Dual inhibition of (V600E)BRAF and the PI3K/AKT/mTOR pathway cooperates to induce apoptosis in melanoma cells through a MEK-independent mechanism. *Cancer Lett*. (2012) 314:244–55. doi: 10.1016/j.canlet.2011.09.037
32. Oskarsson T, Batlle E, Massagué J. Metastatic stem cells: sources, niches, and vital pathways. *Cell Stem Cell*. (2014) 14:306–21. doi: 10.1016/j.stem.2014.02.002
33. Zhang S, Zhou X, Wang B, Zhang K, Liu S, Yue K, et al. Loss of VHL expression contributes to epithelial–mesenchymal transition in oral squamous cell carcinoma. *Oral Oncol*. (2014) 50:809–17. doi: 10.1016/j.oraloncology.2014.06.007
34. Soni S, Padwad YS. HIF-1 in cancer therapy: two decade long story of a transcription factor. *Acta Oncol*. (2017) 56:503–15. doi: 10.1080/0284186X.2017.1301680
35. Wang SC. PCNA: a silent housekeeper or a potential therapeutic target? *Trends Pharmacol Sci*. (2014) 35:178–86. doi: 10.1016/j.tips.2014.02.004
36. Senbanjo IT, Chellaiah MA. CD44: a multifunctional cell surface adhesion receptor is a regulator of progression and metastasis of cancer cells. *Front Cell Dev Biol*. (2017) 5:18. doi: 10.3389/fcell.2017.00018

**Conflict of Interest:** The authors declare that the research was conducted in the absence of any commercial or financial relationships that could be construed as a potential conflict of interest.

Copyright © 2020 Durán-Maldonado, Hernández-Padilla, Gallardo-Pérez, Díaz-Pérez, Martínez-Alcantar, Reyes De la Cruz, Rodríguez-Zavala, Pacheco-Rodríguez, Moss and Campos-García. This is an open-access article distributed under the terms of the Creative Commons Attribution License (CC BY). The use, distribution or reproduction in other forums is permitted, provided the original author(s) and the copyright owner(s) are credited and that the original publication in this journal is cited, in accordance with accepted academic practice. No use, distribution or reproduction is permitted which does not comply with these terms.